

29.6 A 65nm CMOS Hydrogel-Based Dual Fluorescence Sensor for Bioavailable Phosphorus Detection

Ting-Yu Cheng*, Raj S. Mukkamala*, Reinaldo E. Alcalde, Mohamadamin Panahandeh, Akshit Agarwal, Julia A. Kornfield, Dianne K. Newman, Azita Emami

California Institute of Technology, Pasadena, CA

*Equally Credited Authors (ECAs)

Abstract

A hydrogel-based single-culture dual-fluorescence sensor is presented for bioavailable phosphorus (P) detection. The sensor achieves 6.6fA sensitivity with a 15.5dB SNR and an output noise of 1.97mV at 182ms integration time. A large dynamic range is enabled through

high-precision automatic background calibration with a coarse and fine control loop. The sensor was validated using hydrogels embedded with a bioreporter strain and successfully detected both P limitation and cell viability.

Dynamically sensing bioavailable analytes in the environment is currently a very challenging task. For example, phosphorus (P), an essential nutrient for ecosystem health, is typically monitored on active farms at the frequencies of once every several years. Elevated P levels from agricultural runoff can lead to eutrophication in water bodies, while P deficiency in soil limits crop growth and results in economic losses. Traditional methods for water quality tests and soil tests such as Mehlich-3, Olsen, and Bray-P1 procedures [1,2,3] are often expensive and time-consuming. A miniaturized platform based on CMOS technology offers a promising alternative, enabling real-time, low-cost, and high-sensitivity monitoring of environmental chemical levels (Fig. 29.6.1). Fluorescence (FL)-based sensing has emerged as a reliable method due to its selectivity and the ability to report bioavailable responses. Using FL proteins (FPs) expressed in bacteria is more biocompatible and self-sustaining compared to using strong FL sources such as QDots and FL dyes [4,5] for long-term in situ biosensing applications. Prior work [6] monitored FP production using a triple-well microfluidic chamber that requires a separate reference culture to be placed in the center well. Such design needs precise alignment above the sensor and can lead to cell leakage if deployed in soil or water systems. In this work, we use bioengineered bacteria encapsulated in a hydrogel to achieve dual-FL sensing in single culture for simultaneously detecting cell viability and reporting bioavailable P. The proposed integrated CMOS chip enables single-culture single-ended dual-FL measurements with large dynamic range through a high-precision on-chip automatic background calibration. The detection of weak fluorescence signals in the presence of strong scattered excitation background light, exacerbated by the thin geometry of hydrogels, is a major challenge. A feedback loop with coarse and fine control is designed to eliminate the scattered excitation signals with high resolution, thereby enhancing the sensor's dynamic range. Programmable integration time that spans over three orders of magnitude allows the optimum use of the dynamic range of the sensor as higher signal-to-noise ratio (SNR) can be achieved with longer integration time.

Figure 29.6.2 shows the block diagram of the fluorescence sensor. The system integrates on-chip photodiodes (PDs), capacitive transimpedance amplifiers (CTIA), correlated double sampling (CDS) circuits, automatic background calibration, a SAR ADC, a power management unit (PMU), clock generation, LED drivers, and I²C logic for communication with a nRF BLE module enabling future wireless deployment of the sensor in the soil. The targeted bioreporter strain, *Pseudomonas synxantha 2-79*, is encapsulated in a PEGDA (700 Da)/PEGSH (5,000 Da) hydrogel and engineered to express dual FPs: mScarlet-I (RFP) as a constitutive reporter to serve as a proxy for cell viability, and mNeonGreen (GFP) for reporting on the lack of bioavailable P [7]. Dual-band optical filters are used to spectrally separate excitation and emission wavelengths. The emission filter sits atop the CMOS sensor. Excitation LEDs, powered by on-chip LED drivers, illuminate the sample laterally and the dual FL signals are separated via time-multiplexed LED excitation.

Four N+/PW/DNW/P-sub triple junction PDs, 800um x 600um each, are employed as the sensing elements. These PDs are connected to two sets of CTIA and CDS readout circuits. Low-leakage switches are used to interface the PDs with the CTIA inputs. Additionally, dark PDs are connected to the opposite side of the CTIA differential input to partially cancel the dark photocurrent. The CTIA incorporates a 7-bit binary-weighted capacitive feedback network, with the MSB corresponding to a feedback capacitance of 138.56fF. The sensor exhibits linear response across varying input light power, as well as at different integration times under a fixed input power, as shown in Fig. 29.6.3. The readout circuits achieve a minimum detectable front-end current of 6.6fA with a SNR of 15.5dB (Fig. 29.6.4.). The responsivity of the on-chip PDs is measured to be 9.97mA/W at a wavelength of 600nm. The root-mean-square output noise of the sensor under dark conditions is 1.97mV at an integration time of 182ms. A SAR ADC [8] is used to digitize the CDS output, and the resulting data is transmitted over I²C for logging and further analysis.

The emission intensity of fluorescence proteins is governed by equation (1): $I_{FL} = QY \times I_{EX} \times (1 - 10^{-EC \times CL})$, where QY is the quantum yield of the target FP, EC is the extinction coefficient, C is the concentration of the fluorophores, and L is the optical path length. For a 10pM mScarlet-I sample with a 1mm optical path length for miniaturized environmental sensors, the excitation-to-emission intensity ratio is greater than 10⁶. In addition, since the excitation background varies depending on environmental conditions, concentration of cells, and material being used in the encapsulates, the background signal is difficult to precisely

predict. The background mainly arises from stray and reflected LED excitation light, as well as scattered light from interaction with the samples, which can easily saturate the FL sensor. To address this, two 9-bit current DACs were implemented for coarse and fine tuning, with maximum output currents of 93pA and 1.65pA, respectively. The outputs of both DACs are summed to generate the VCCS compensation current. The output current range can be further adjusted by selecting one of four available gate voltages (V_{G1}), ranging from 1.45-to-1.6V for coarse control and 1.5-to-1.65V for fine control, to account for process variations. As characterized in Fig. 29.6.3, the measured waveforms using the FL sensor show good agreement with simulation results. Two operating modes are designed for VCCS control: (1) automatic mode and (2) manual mode. In automatic mode, a comparator is used to detect the polarity of the CDS differential output. When the output is positive, the 9-bit counter steps up until the polarity flips. The control logic next reverts the previous count, holds the value for the coarse-tuning current DAC, and starts the next counter for fine-tuning current DAC until the polarity flips again. Figure 29.6.4 demonstrates the calibration process conducted prior to FL measurements using a hydrogel embedded with a dual reporter strain. Calibration was activated at the beginning of the measurement before the hydrogel started to produce significant FL signal. Calibration was performed sequentially for each set of readout circuits with the corresponding excitation LED illuminated. The noticeable excitation background occupying most of the dynamic range was reduced gradually as the automatic closed-loop circuitry began the calibration process, until the effect of background was minimized. The dual reporter FL responses were recorded next. The simulated worst-case VCCS resolutions, which occur at the steepest regions of the characteristic curves, are 500fA for coarse tuning and 22fA for fine tuning. The manual mode is done by sending external commands via the nRF BLE module to overwrite the 9-bit control registers through I²C communication. To further suppress stray light, the chip employs metal shielding around all photodiodes using metal layers M1–M7. This prevents sidewall light leakage through the 0.3mm thick die.

Band-gap reference circuits are used to generate stable reference voltages and currents across the chip. Multiple LDOs provide regulated supply voltages of 1.8V, 1.2V, 1V and 0.5V to power the core FL sensing circuits, readout chain, and all the other on-chip circuitry. Because the absolute FL intensity is primarily estimated through theoretical calculations using equation (1), and can vary due to sample geometry, optical coupling efficiency and biological factors such as cell growth, the integration time is highly programmable. The clock generation circuits support integration times from 6ms to 24.6s, enabling signal detection across a wide dynamic range. A current-starved ring oscillator generates a base frequency of 340kHz. This clock is used for generating CLK1-CLK4 through a clock phase generator with unit delay elements to create timing difference in controlling the readout circuits. CLK5 with a 90-degree phase shift is used for digital calibration logic, ensuring it queries the CDS output only after charge redistribution is fully completed.

The sensor was tested with bacterial cells contained within hydrogels. The hydrogels were prepared by encapsulating the dual reporter strain engineered to express GFP under P-limited conditions and RFP constitutively to indicate cell viability and growth. The hydrogels were transferred onto 25mm x 25mm No. 1 coverslips for sensor measurements. Two sample groups were tested 24 hours after gel preparation: (1) hydrogels preloaded with 0.5mM phosphate (P-limited) and (2) those preloaded with 5mM phosphate (P-replete). The sensor successfully detected P limitation by distinguishing between the two conditions (Fig. 29.6.5. (top)). In order to verify the results, wild-type (WT) samples, which contain bacteria without FPs, were also measured, and net FL signals were calculated by subtracting the signals of WT samples from the bioreporter samples. A clear signal difference was seen in the green channel, with P-limited samples exhibiting stronger signals than the P-replete samples. In contrast, the red channel showed similar signal levels for both groups, indicating comparable cell loading and growth. The sensor can also monitor cell growth and nutrient response over time under aqueous environments. For these experiments, a well filled with phosphate solution, matching the gel's phosphate concentration, was placed on each hydrogel to maintain a controlled nutrient environment. According to prior characterization [7], the bioreporter activates GFP expression when the phosphate concentration is consumed below 50uM by cells. The time resolved response (Fig. 29.6.5. (bottom)) showed a GFP signal induction in the P-limited sample after 10 hours of experiment, indicating phosphate depletion, while the P-replete counterpart showed no induction. RFP signals were constitutively expressed in both samples, suggesting active cell viability.

The comparison table and the die micrograph implemented in 65nm CMOS are shown in Fig. 29.6.6 and Fig. 29.6.7, respectively. To the best of our knowledge, this is the first FL chip that detects dual-FL signals from a single-culture bioreporter for monitoring bioavailable P using hydrogel encapsulates. The small size, large dynamic range, low power, and hydrogel-based design enables miniaturized wireless sensors for applications in environmental sensing and precision agriculture through real-time monitoring of analyte bioavailability.

Acknowledgement:

This work was supported by the Resnick Sustainability Institute at Caltech and the Institute for Collaborative Biotechnologies. The authors would like to thank them for their generous funding that made this research possible.

References:

[1] H. Zhang *et al.*, "Interlaboratory validation of the Mehlich 3 method for extraction of plant-available phosphorus". *J AOAC Int.*, 2009 Jan-Feb;92(1):91-102. <https://doi.org/10.1093/jaoac/92.1.91>

[2] M.d.C. Horta, J. Torrent, "The Olsen P method as an agronomic and environmental test for predicting phosphate release from acid soils". *Nutr Cycl Agroecosyst* 77, 283–292 (2007). <https://doi.org/10.1007/s10705-006-9066-2>

[3] A.M. Ebeling, L.G. Bundy, A.W. Kittell and D.D. Ebeling, "Evaluating the Bray P1 Test on Alkaline, Calcareous Soils". *Soil Sci. Soc. Am. J.*, 72: 985-991, 2008. <https://doi.org/10.2136/sssaj2006.0347>

[4] C. Zhu *et al.*, "An Ingestible Pill with CMOS Fluorescence Sensor Array, Bi-Directional Wireless Interface and Packaged Optics for in-Vivo Bio-Molecular Sensing," *IEEE Transactions on Biomedical Circuits and Systems*, vol. 17, no. 2, pp. 257-272, April 2023. <http://doi.org/10.1109/TBCAS.2023.3244570>

[5] M. Roschelle *et al.*, "A Wireless, Multicolor Fluorescence Image Sensor Implant for Real-Time Monitoring in Cancer Therapy," *IEEE Journal of Solid-State Circuits*, vol. 59, no. 11, pp. 3580-3598, Nov. 2024. <http://doi.org/10.1109/JSSC.2024.3435736>

[6] F. Aghlmand *et al.*, "A 65-nm CMOS Fluorescence Sensor for Dynamic Monitoring of Living Cells," *IEEE Journal of Solid-State Circuits*, vol. 58, no. 11, pp. 3003-3019, Nov. 2023. <http://doi.org/10.1109/JSSC.2023.3308853>

[7] E.M. Larsson, R.M. Murray, D.K. Newman, "Engineering the Soil Bacterium *Pseudomonas synxantha* 2–79 into a Ratiometric Bioreporter for Phosphorus Limitation". *ACS Synth. Biol.* 2024, 13, 1, 384–393. <https://doi.org/10.1101/2023.10.20.563366>

[8] S. Sharma *et al.*, "A Monolithic 3D Magnetic Sensor in 65nm CMOS with <math><10\mu\text{Trms}</math> Noise and 14.8 $\mu\text{W}</math> Power," *IEEE Custom Integrated Circuits Conference (CICC)*, 2023, pp. 1-2. <http://doi.org/10.1109/CICC57935.2023.10121313>$

[9] A. Manickam *et al.*, "A Fully Integrated CMOS Fluorescence Biochip for DNA and RNA Testing," *IEEE Journal of Solid-State Circuits*, vol. 52, no. 11, pp. 2857-2870, Nov. 2017. <http://doi.org/10.1109/JSSC.2017.2754363>

[10] Q. Liu *et al.*, "A Threshold-Based Bioluminescence Detector With a CMOS-Integrated Photodiode Array in 65 nm for a Multi-Diagnostic Ingestible Capsule," *IEEE Journal of Solid-State Circuits*, vol. 58, no. 3, pp. 838-851, March 2023. <http://doi.org/10.1109/JSSC.2022.3197465>

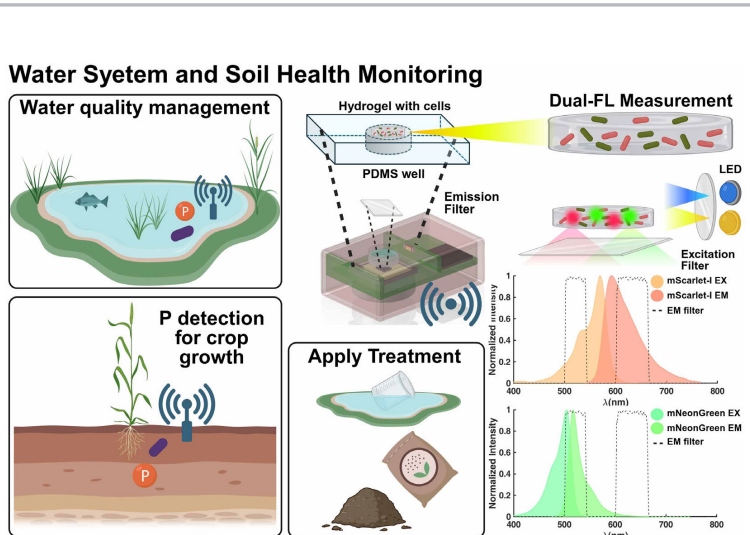


Figure 29.6.1: Integrated dual fluorescence sensor with bioreporter encapsulated in hydrogels and its applications.

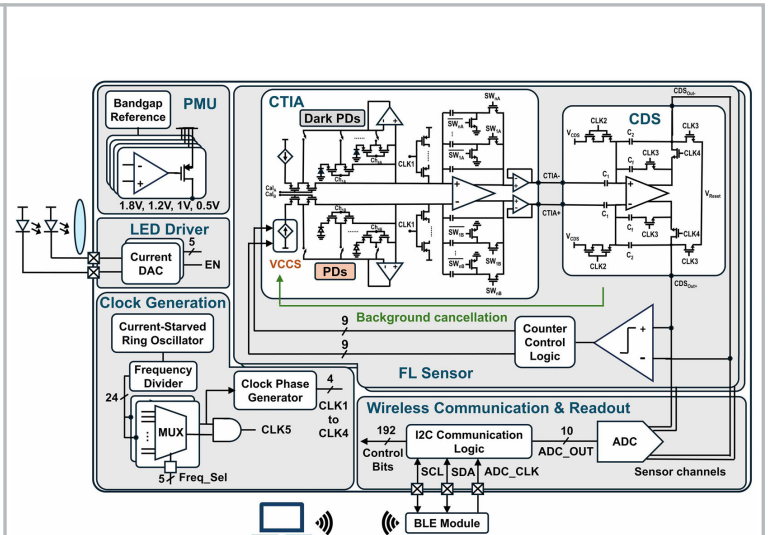


Figure 29.6.2: Block diagram of the wireless dual fluorescence sensor.

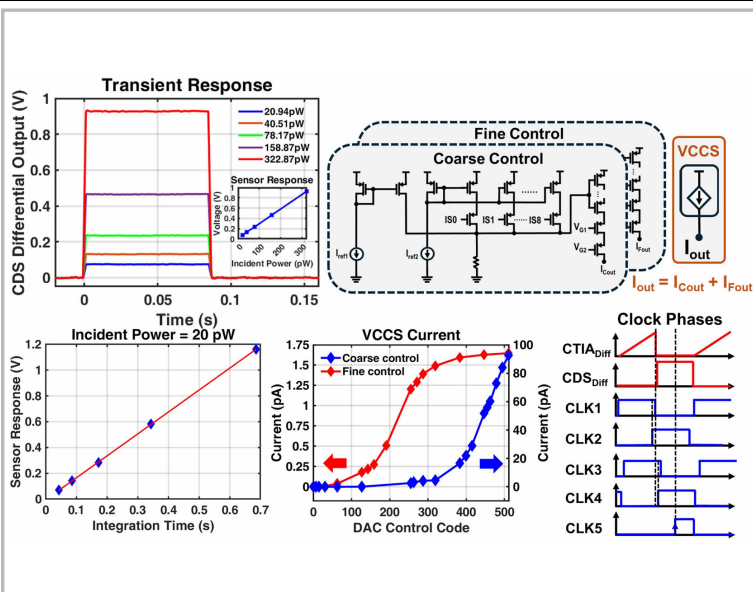


Figure 29.6.3: Sensor responses, VCCS circuit and current, and clock phases for sensor readout.

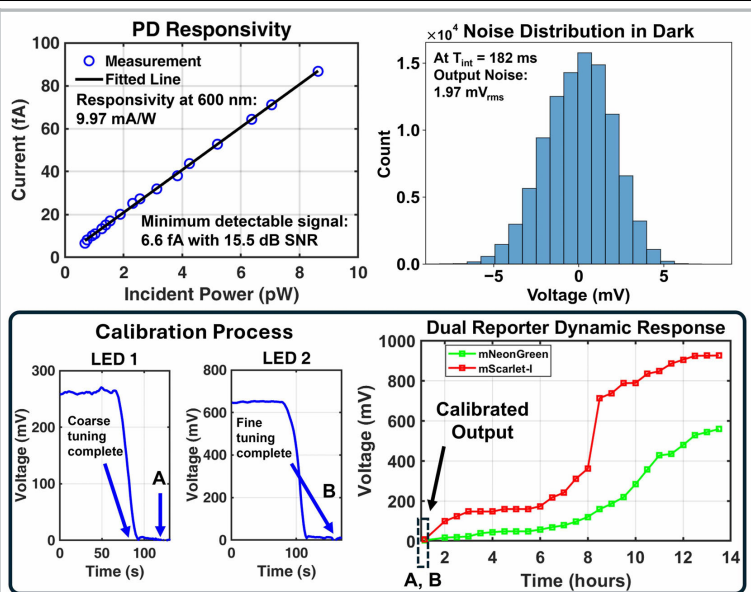


Figure 29.6.4: Photodiode responsivity, noise under dark condition, and background calibration process.

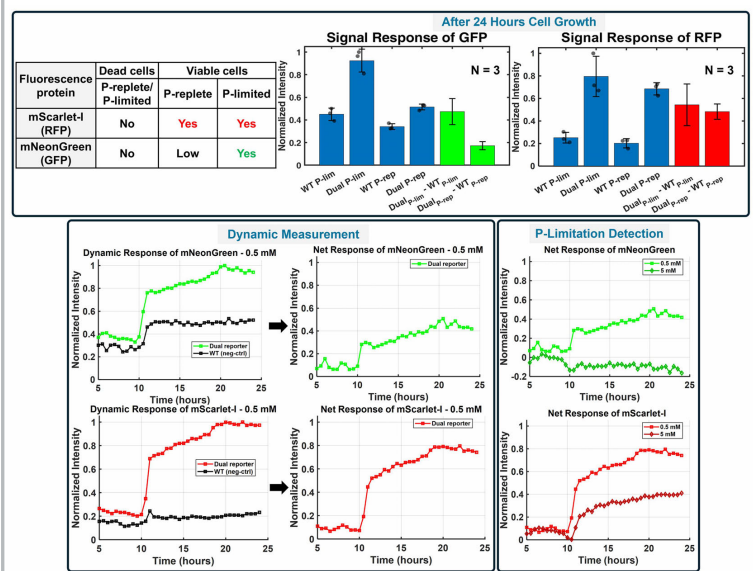


Figure 29.6.5: Static and dynamic measurements of hydrogels showing signal induction under P-limited condition.

Metric	JSSC 2017 [9]	JSSC 2022 [10]	TBioCAS 2023 [4]	JSSC 2023 [6]	JSSC 2024 [5]	This Work
Technology	250 nm CMOS	65 nm CMOS	65 nm CMOS	65 nm CMOS	180 nm CMOS	65 nm CMOS
Application	DNA/RNA testing	Biochemical detection	Bio-molecular sensing	Dynamic cell monitoring	Imaging of treatment response	Bioavailable P detection
Detector Type	Fluorescence	Bioluminescence	Fluorescence	Fluorescence	Fluorescence	Fluorescence
Reporter Type	DNA/RNA	In vitro bioengineered bacterial sensors	In vitro DNA assay	Fluorescence proteins in E. coli bacteria	Ex vivo immune cells	Rhizosphere bacteria encapsulated in hydrogels
Excitation/Emission Peak (nm)	490~580	N/A	405/800 (QDot800)	387/703 (mRFP), 437/573 (LSSmOrange), 586/610 (mCherry), ~515~530 (sYFP)	455/500 (FAM), 650/670 (Cy5), 785/800 (beads)	505/517 (mNeonGreen), 570/594 (mScarlet-I)
Measurement Type	Static	Static / Dynamic	Static	Static/Dynamic	Static	Static / Dynamic
Excitation Source	LED	N/A	UV LED	SMD LED	Laser diode	SMD LED
Supply Voltage	2.5 V	2.5 V	N/R	3.3 V	5.5 V*	2 V
Chip Size	63 mm ²	14.9 mm ²	4 mm ²	3 mm ²	12.5 mm ²	5 mm ²
Output Noise*	N/R	N/R	1~2 mV (Photon shot noise), 0.4 mV (CTIA)	3.846 mV _{rms}	5.4 mV	1.97 mV _{rms}
SNR	> 20 dB	N/R	1	18.3 dB	20 dB**	15.5 dB
Sensor Sensitivity	~10fA	59 fA	40 dots/μm ²	1.05 fA	N/R	6.6 fA
On-Chip Excitation Background Removal	No	N/A	No	Yes**	No	Yes
Integration Time	N/R	25.8 s	N/R	1 s	0 ms - 248 ms	6 ms - 24.6 s
Power	118 mW	16.3 uW	1.4 mW	7.05 mW [†]	2.09 mW	1.66 mW

N/A: Not applicable, N/R: Not reported, * Under dark condition, ** T_{int} = 98 ms
 † Remains at 5.5 V throughout imaging and drops to 3.5 V during readout. ‡‡ Manual control
 § One row: include CTIA + 4 buffers + 1/3 of a shared CDS for 4 pixels

Figure 29.6.6: Comparison table of state-of-the-art fluorescence sensors.

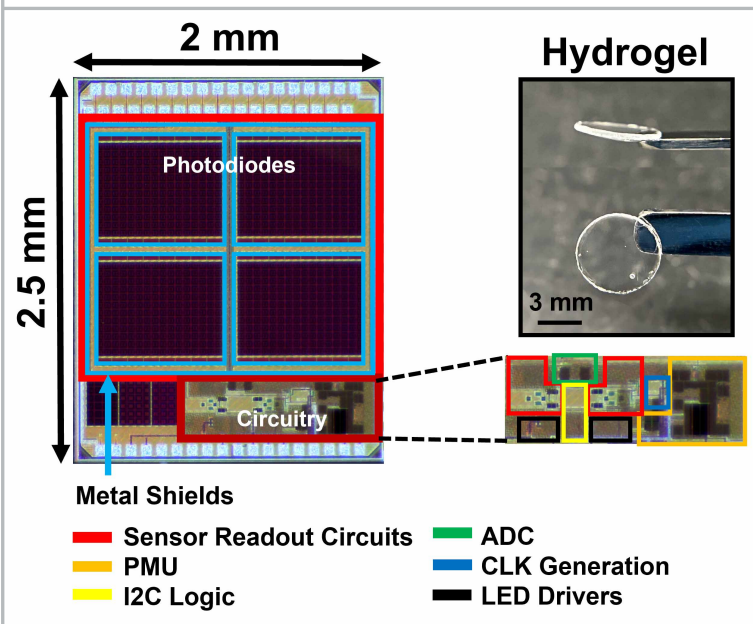


Figure 29.6.7: Die micrograph and photo of hydrogels used in biological experiments.